

## Supporting Information

### **Flexible and transparent sensors for ultra-low NO<sub>2</sub> detection at room temperature under visible lights**

*Xiao-Xue Wang<sup>a</sup>, Hua-Yao Li<sup>\*b</sup> and Xin Guo<sup>\*a</sup>*

*<sup>a</sup> State Key Laboratory of Material Processing and Die & Mould Technology, Laboratory of Solid State Ionics, School of Materials Science and Engineering, Huazhong University of Science and Technology, Wuhan 430074, P. R. China*

*<sup>b</sup> School of Optical and Electronic Information, Huazhong University of Science and Technology, Wuhan 430074, P. R. China*

*\*Author to whom correspondence should be addressed. Email: [xguo@hust.edu.cn](mailto:xguo@hust.edu.cn);  
[huayaoli@hust.edu.cn](mailto:huayaoli@hust.edu.cn)*

### **Fabrication of array of parallel $\text{In}_2\text{O}_3$ nanowires by electrospinning**

The prepared precursor solution was transferred into a plastic syringe for electrospinning. The precursor was electrospun from a stainless-steel needle (21 gauge with orifice diameter of 0.5 mm) onto the PI substrate (Hylimide®STPI370, 20  $\mu\text{m}$ ) laying on a specially-designed collector consisting of two pieces of parallel copper electrodes separated by a 13 mm gap and placed 100 mm below the needle tip. A DC voltage of 10 kV was applied between the needle and the collector. During the electrospinning process, the precursor was continuously fed using a syringe pump at a rate of 0.03 mm/min and the electrospinning time was limited to 120 s. The ambient temperature and humidity for the electrospinning were kept at 25 °C and 30%, respectively. Assisted by electrostatic interactions, the electrospun wires were stretched on the PI substrate to form arrays of parallel nanowires. Fig. S1 illustrates the setup of the electrospinning.

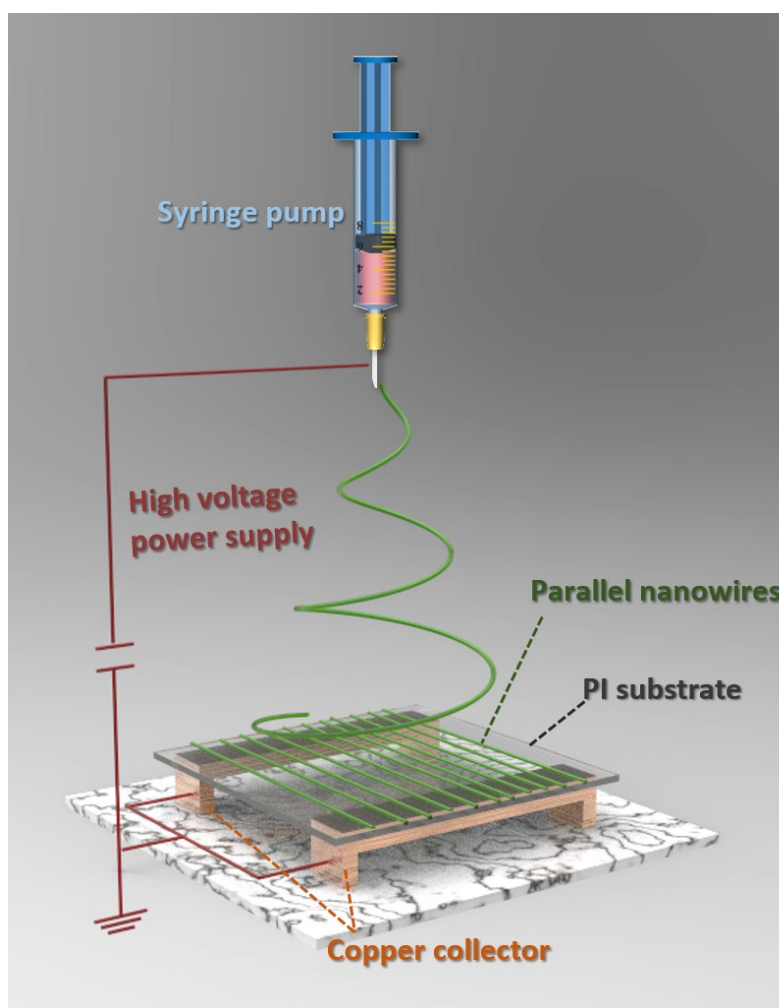


**Fig. S1.** Schematic illustration of the electrospinning setup.

### Characterization of In<sub>2</sub>O<sub>3</sub> nanowires

TEM image of the In<sub>2</sub>O<sub>3</sub> nanowires (Fig. S2) reveals that the In<sub>2</sub>O<sub>3</sub> nanowires are surrounded by the organic residue of unburned PVP, which agrees with the FFT (Fast Fourier Transform) pattern given in the inset of Fig. S2 (b). According to Fig. S2, the size of In<sub>2</sub>O<sub>3</sub> nanoparticles in the nanowires is ca. 5-10 nm with an average interplanar spacing of ~0.292 nm, being consistent with the (222) *d*-space of cubic In<sub>2</sub>O<sub>3</sub>. The EDX pattern in Fig. S3 confirms the presence of carbon in the In<sub>2</sub>O<sub>3</sub> nanowires.

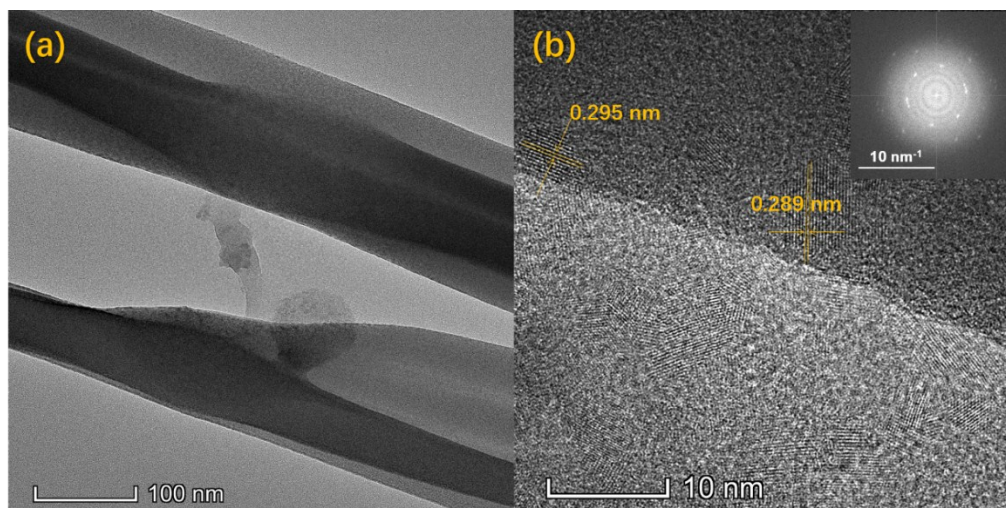


**Fig. S2.** TEM images of In<sub>2</sub>O<sub>3</sub> nanowires.

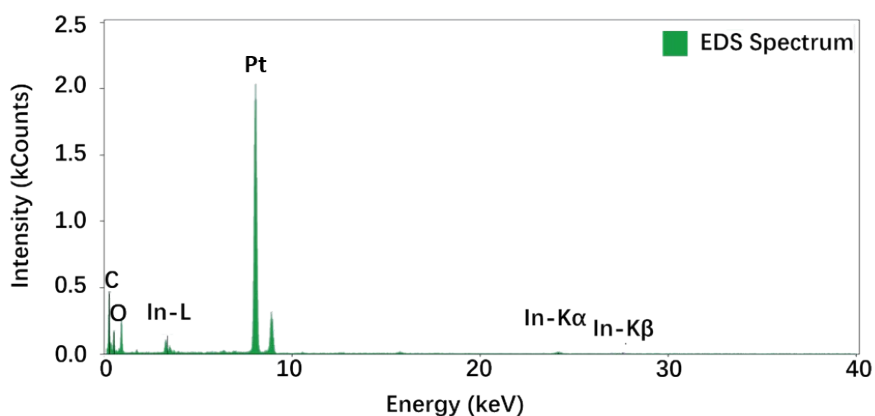


**Fig. S3.** EDX pattern of In<sub>2</sub>O<sub>3</sub> nanowires.

The highest EDX peak is Pt, which was coated on the sample surface for better imaging.

### Effect of light irradiance on gas-sensing performance

The responses of the  $\text{In}_2\text{O}_3$  nanowire sensor to  $\text{NO}_2$  under blue light with different irradiances are shown in Fig. S4. As the irradiance increases from 5.1 to 53.6  $\text{W}/\text{m}^2$ , the recovery time decreases while the responses are almost constant, demonstrating that the sensor is not sensitive to the light intensity, which is advantageous for situations of varying lighting.

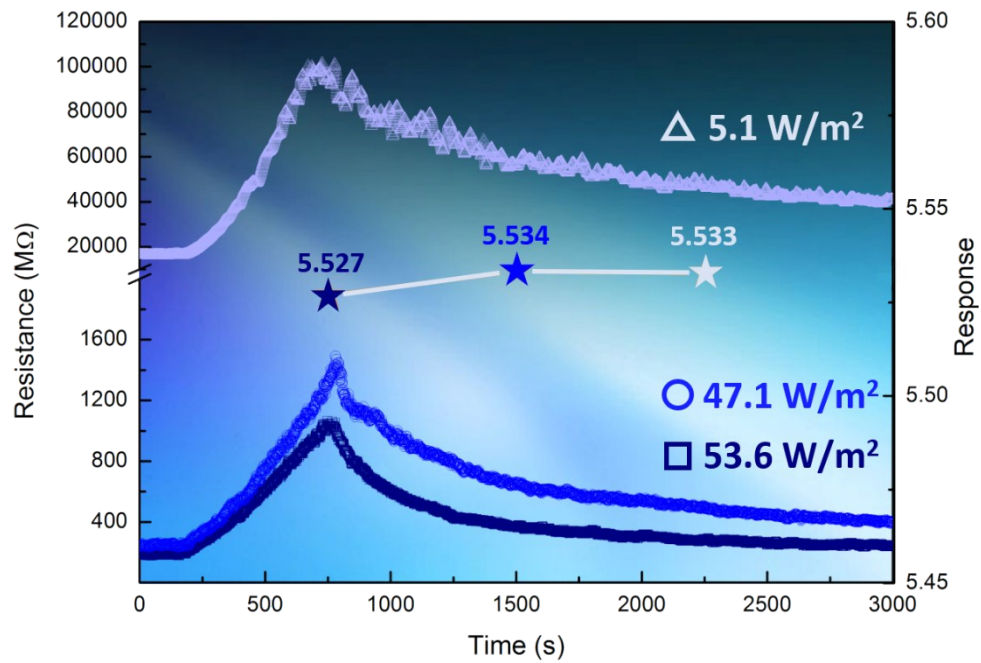


**Fig. S4.** Response-recovery curve and response of the sensor to 500 ppb  $\text{NO}_2$  under blue LED with different irradiances.

### Effect of humidity on the gas-sensing performance

The responses of the  $\text{In}_2\text{O}_3$  nanowire sensor to humidity under the white light illumination are exhibited in Fig. S5(a). The relative humidity is varied from 10 to 60%, but the responses to humidity are rather small ( $R = 1.2$ - $1.25$ ), as compared with the response to 500 ppb  $\text{NO}_2$  in Fig. 3(e) ( $R = 7.08$ ). The relative change ( $S_{(\text{NO}_2 \text{ in humidity})}/S_{(\text{NO}_2 \text{ in dry air})}$ ) of the sensor response to 500 ppb  $\text{NO}_2$  brought about by humidity is presented in Fig. S5(b). Although slight changes are observed in the humid atmospheres, the relative changes are quite small as compared with the high response values. Therefore, the  $\text{In}_2\text{O}_3$  nanowire sensor can effectively detect  $\text{NO}_2$  in humid ambient atmospheres.

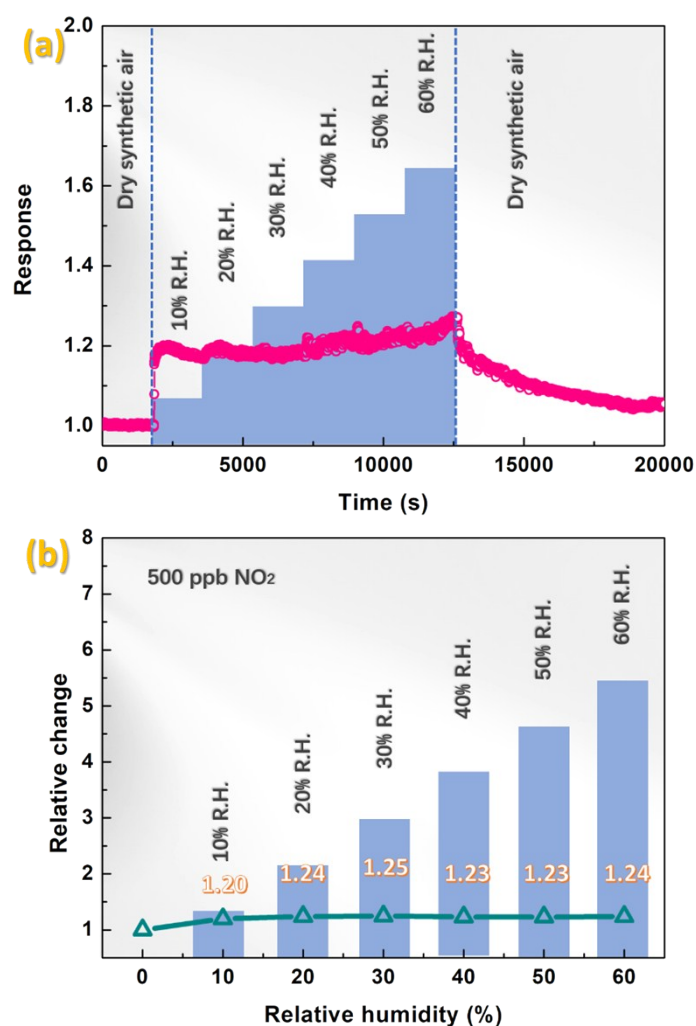


**Fig. S5.** (a) Response-recovery curve of the sensor to humidity under the white LED illumination. (b) Relative change ( $S_{(\text{NO}_2 \text{ in humidity})}/S_{(\text{NO}_2 \text{ in dry air})}$ ) of the sensor response to 500 ppb  $\text{NO}_2$  brought about by humidity under the white LED illumination.

## Optical characterization of LED light sources

**Table S1.** Irradiances of various LED light sources and iPhone screen

Light	Blue	White	Green	Red	iPhone
Irradiance W/m <sup>2</sup>	53.6	100.0	12.3	29.3	0.56

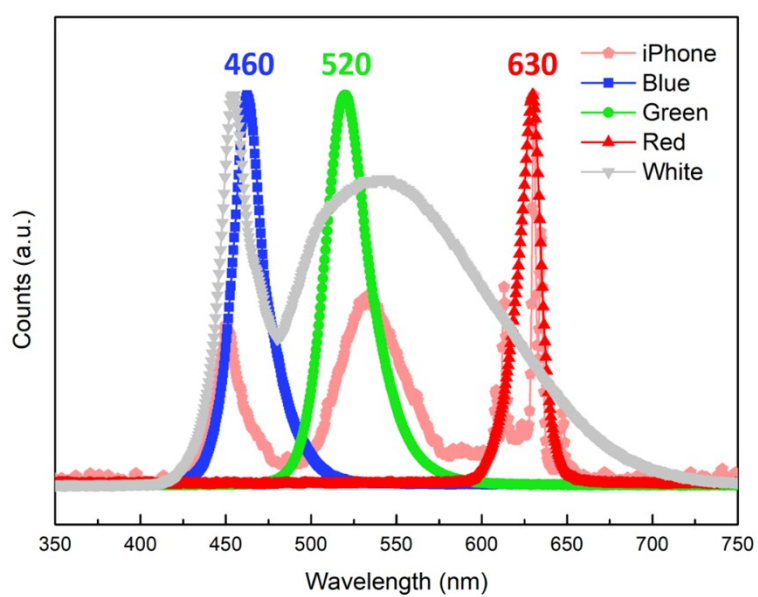


**Fig. S6.** Wavelength spectra of four LEDs and iPhone screen.

## Sensor response and recovery time

**Table S2.** Gas sensing properties of the In<sub>2</sub>O<sub>3</sub> nanowire sensor.

Light	Target gas	Concentration (ppb)	Response	Recovery time (s)
Blue	NO <sub>2</sub>	500	5.52	1100
Blue	NO <sub>2</sub>	10	1.14	989
White	NO <sub>2</sub>	500	7.08	1202
White	NO <sub>2</sub>	10	1.23	1280

## Gas-sensing performance under the iPhone screen illumination

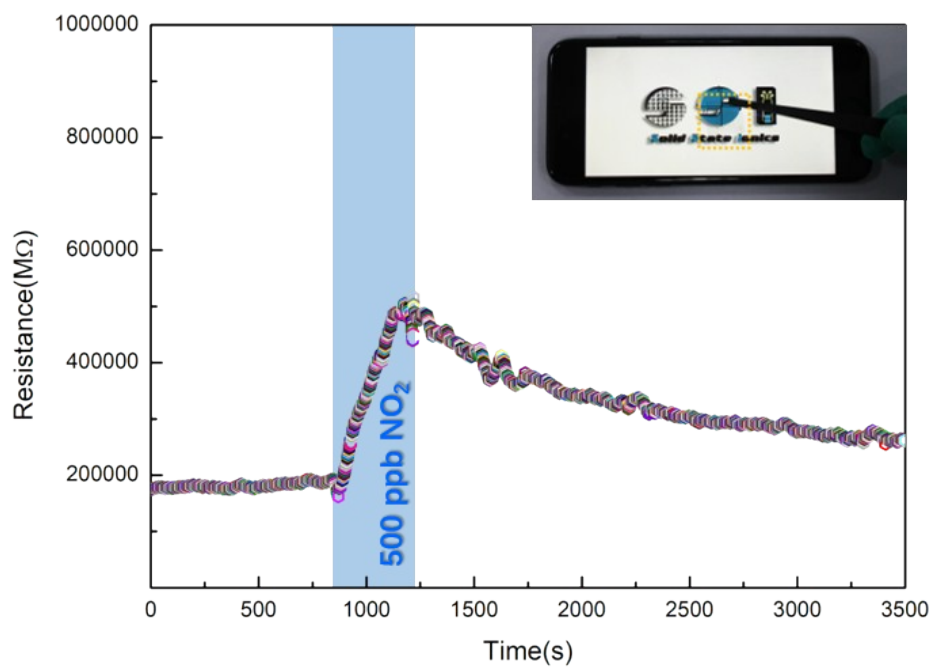


**Fig. S7.** Response-recovery curve of the sensor to 500 ppb NO<sub>2</sub> under phone screen illumination (iPhone 7, 100% luminance) at room temperature.

**UV-Vis absorption**

UV-Vis absorption spectrum (Fig. S8 (a)) was applied to characterize the optical band gap of the  $\text{In}_2\text{O}_3$  nanowire array, and the value was determined to be 1.523 eV from the intercept in the Tauc Plot (Fig. S8 (b)).

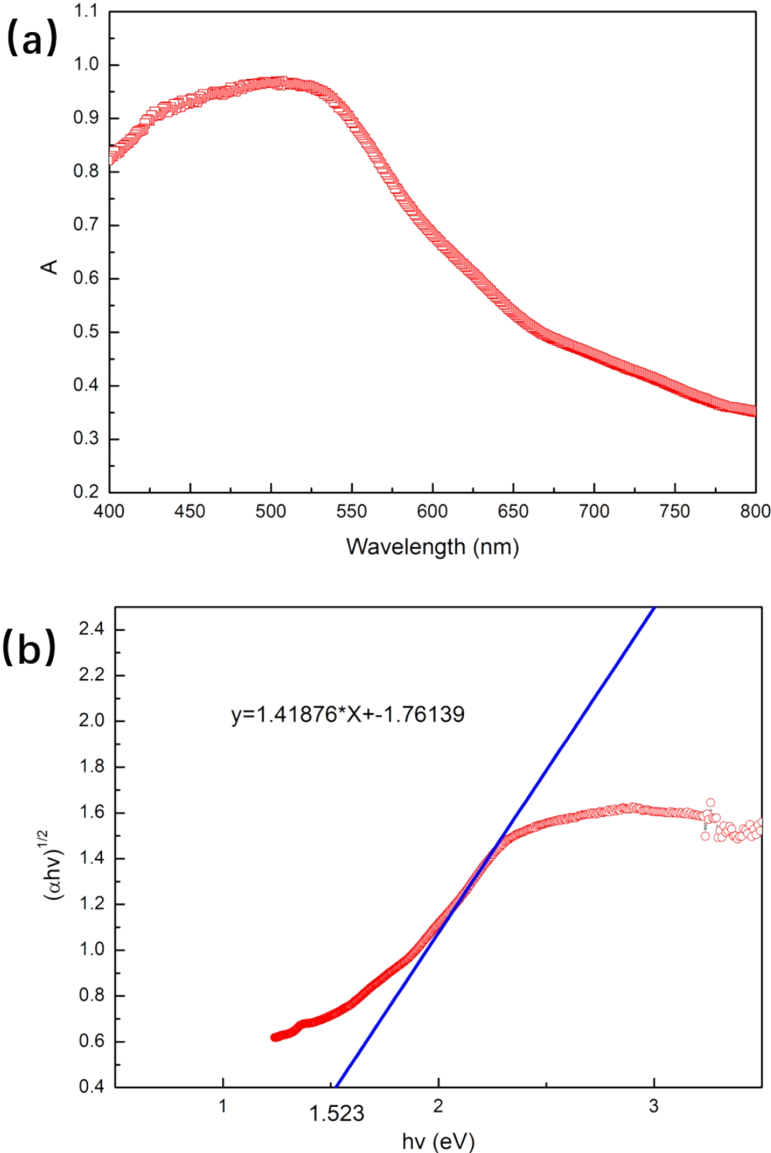


**Fig. S8.** UV-vis absorption spectrum of the  $\text{In}_2\text{O}_3$  nanowire array.

## DFT calculations

First principles were employed to describe the reactions with the projector augmented wave (PAW) method based on DFT. The exchange-functional was treated using the generalized gradient approximation (GGA) of the Perdew-Burke-Ernzerhof (PBE) functional. The energy cutoff for the plane wave basis expansion was set to be 400 eV, and the force on each atom was set to be less than 0.03 eV/Å for the convergence criterion of the geometry relaxation. For the surface structure, a  $3 \times 3 \times 1$  Monkhorst and Pack  $k$ -point sampling was employed. The crystal structure models are shown in Fig. S9 (a) and (b) and the band structures of pure  $\text{In}_2\text{O}_3$  and  $\text{In}_2\text{O}_3$ /carbon composite are shown in Fig. S9 (c) and (d).

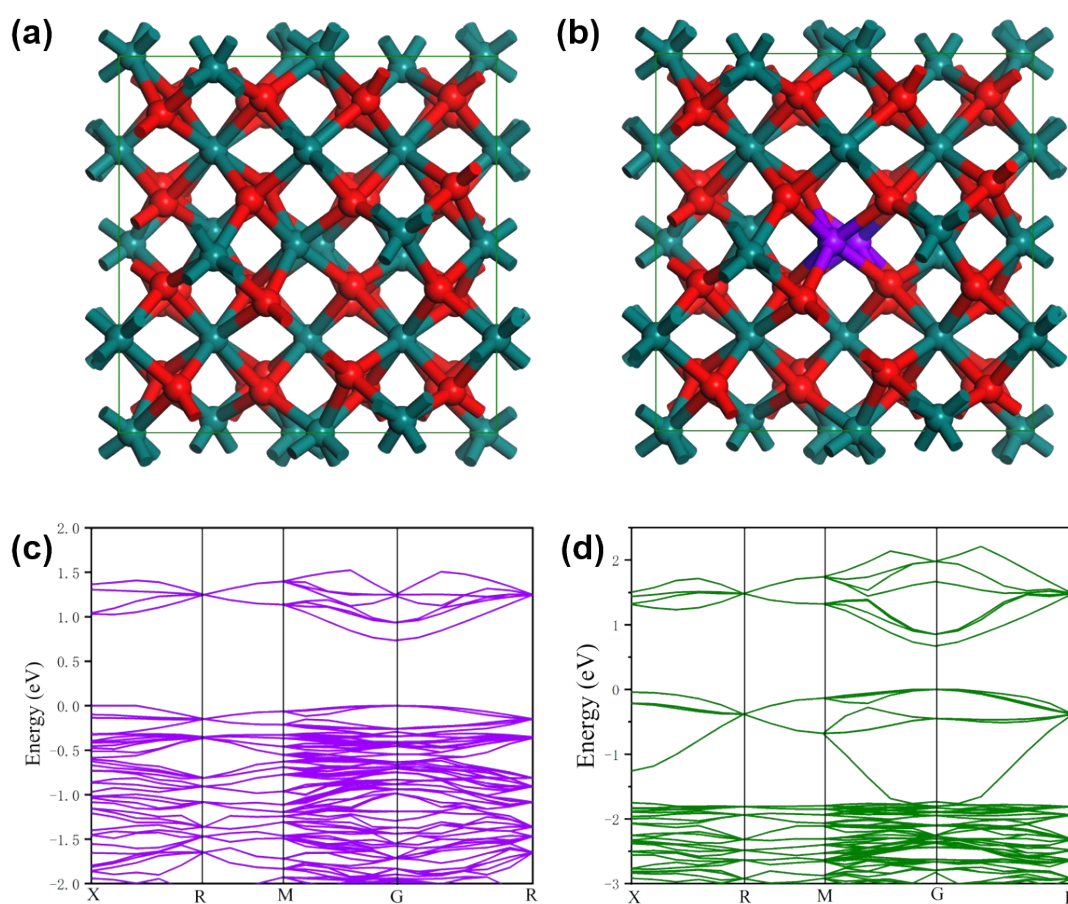


**Fig. S9.** Crystal structures (cubic structure, space group:  $la3$ ) of (a) the pure  $\text{In}_2\text{O}_3$  and (b) the  $\text{In}_2\text{O}_3$ /carbon composite, and the band structures of (c) the pure  $\text{In}_2\text{O}_3$  and (d) the  $\text{In}_2\text{O}_3$ /carbon composite (Red atoms: Oxygen; Navy blue atoms: Indium; Purple atoms: Carbon). The bandgap of the  $\text{In}_2\text{O}_3$ /carbon composite (0.6 eV, as determined from the DFT calculation) is lower than that of the pure one (0.9 eV), benefiting the light absorption.